Orbital Disorder Induced by Charge Fluctuations in Vanadium Spinels

Yasuyuki Kato, Gia-Wei Chern, K. A. Al-Hassanieh, Natalia B. Perkins, and C. D. Batista

Phys. Rev. Lett. **108**, 247215 — Published 15 June 2012

DOI: 10.1103/PhysRevLett.108.247215

Orbital disorder induced by charge fluctuations in vanadium spinels

Yasuyuki Kato,[1] Gia-Wei Chern,[2,3] K. A. Al-Hassanieh,[2,4] Natalia B. Perkins,[3] and C. D. Batista[1]

[1] *Theoretical Division, T4 and CNLS, Los Alamos National Laboratory, Los Alamos, New Mexico 87545, USA*
[2] *Theoretical Division, Los Alamos National Laboratory, Los Alamos, New Mexico 87545, USA*
[3] *Department of Physics, University of Wisconsin, Madison, Wisconsin 53706, USA*
[4] *Center for Nanophase Materials Sciences, Oak Ridge National Laboratory, Oak Ridge, Tennessee 37831, USA*

Motivated by recent experiments on vanadium spinels, AV_2O_4, that show an increasing degree of electronic delocalization for smaller cation sizes, we study the evolution of orbital ordering (OO) between the strong and intermediate-coupling regimes of a multi-orbital Hubbard Hamiltonian. The underlying magnetic ordering of the Mott insulating state leads to a rapid suppression of OO due to enhanced charge fluctuations along ferromagnetic bonds. Orbital double-occupancy is rather low at the transition point indicating that the system is in the crossover region between strong and intermediate-coupling regimes when the orbital degrees of freedom become disordered.

PACS numbers: 75.10.Jm, 75.30.Et, 75.50.Ee

The steady interest in frustrated magnets with degenerate orbitals is driven by the continuous discovery of unusual magnetic and orbital orderings resulting from an intricate interplay between frustration, lattice distortions and electron correlations. A case in point is the family of vanadium spinels, AV_2O_4 (A = Cd, Mg or Zn), whose magnetic V^{3+} ions reside on a pyrochlore lattice and contain two electrons in their t_{2g} $3d$-orbitals [1–5]. What makes this family particularly attractive is the possibility of tuning the ratio between the electronic hopping, t, and the intra-orbital Coulomb repulsion, U, by changing the cation size at A sublattice [6].

By using a strong-coupling approach, Tsunetsugu and Motome found an antiferro-orbital (AFO) order consisting of alternating d_{zx} and d_{yz} orbitals along both $[1, 0, \pm 1]$ (zx) and$[0, 1, \pm 1]$ (yz) directions [7]. However, AFO is incompatible with the crystal symmetry $I4_1/amd$ extracted from neutron scattering (NS) and x-ray diffraction experiments [1–3]. Tchernyshyov [8] proposed that AFO is suppressed by a strong spin-orbit (SO) interaction [8–10]. Although there is no reliable data on the SO coupling for V^{3+} ions, free ion measurements [11] and *ab initio* calculations [12] indicate that it may be comparable to the exchange energy. However, recent NS measurements on MgV_2O_4 [3] detected a small spin gap and highly dispersive magnetic excitations that are at odds with strong SO coupling [13]. More recent experimental studies of the AV_2O_4 family show that none of these compounds satisfy the phenomenological Bloch's equation [14] $\partial \ln T_N / \partial \ln V \simeq 3.3$, that must hold in the strong-coupling limit $t/U \ll 1$ [6] (T_N and V are Néel temperature and volume). Moreover, the Néel temperature of ZnV_2O_4 decreases with pressure and transport measurements reveal that MgV_2O_4 and ZnV_2O_4 have small charge gaps [15]. These measurements clearly indicate that a comprehensive study of the spinel vanadates requires an approach that can interpolate between the strong and intermediate-coupling regimes.

In this Letter we demonstrate that the larger charge fluctuations of the intermediate-coupling regime play a crucial role for suppressing OO in MgV_2O_4 and ZnV_2O_4. The observed magnetic ordering breaks the equivalency between bonds and the strong Hund's coupling results in a lower energy barrier for ferromagnetic (FM) bonds. Since the FM bonds form zig-zag chains spiraling along the z direction (see Fig. 1), charge fluctuations become stronger along these chains. We argue that it is essential to keep double occupied states in the low-energy effective theory to account for the lower energy barrier of FM bonds. In fact, we show that double occupied states of isolated zig-zag chains are domain walls of a 1D quantum Ising model. These domain walls are confined in the orbitally ordered phase. As t/U increases, the zig-zag chain undergoes a quantum phase transition to a para-orbital (PO) [16] state via proliferation of domain walls. We find that this transition takes place at the crossover between the intermediate and strong-coupling regimes. This phenomenon cannot be captured by a strong-coupling approach because double-occupied states are projected out from the low-energy Hilbert space.

We first review experimental results on vanadium spinels. A structural transition occurs at a temperature $T_s \approx 95$K for A = Cd [4, 5], $T_s \approx 51$K for A = Zn [2], and $T_s \approx 65$K for A = Mg [3], which lowers the crystal symmetry from cubic $Fd\bar{3}m$ to tetragonal $I4_1/amd$ and leads to uniform flattening of VO_6 octahedra with $c < a = b$. This distortion leads to a partial ferro-orbital (FO) ordering in which the lower-energy d_{xy} orbital is occupied at every site, while the second electron can occupy either the d_{zx} or d_{yz} orbitals. Antiferromagnetic correlations develop below T_s along chains parallel to $[1, \pm 1, 0]$ (xy) directions. However, 3D magnetic ordering only sets in below a lower Neel temperature due to frustration in the inter-chain coupling. The ordering wave-vector is $\mathbf{q} = 2\pi(0, 0, 1)$ and the corresponding spin pattern is $\uparrow\uparrow\downarrow\downarrow$ along chains parallel to the yz or zx directions. This ordering leads to zig-zag FM chains spiraling about the z-axis (Fig. 1).

The Model. We start by considering a low-energy t_{2g} Hamiltonian $H = H_{cf} + H_U + H_t + H_{so}$. The first term, $H_{cf} = -\Delta \sum_j n_{j\,xy}$, describes the crystal field splitting due to the Jahn-Teller distortion at $T < T_s$, where $n_{j\,xy}$

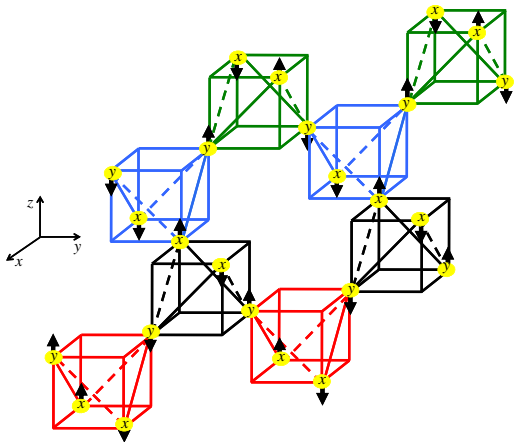

FIG. 1: (Color online) Pyrochlore lattice of V^{3+} ions in AV_2O_4. The solid diagonal lines are FM bonds along zx and yz directions. These "strong" bonds form zig-zag chains described by $\bar{H}$. The dashed lines are the "weak" AFM bonds that introduce inter-chain orbital coupling. The arrows indicate the spin ordering favoured by a combination of the intra-chain FM coupling and inter-chain AFM coupling induced by bonds oriented along the xy direction. The letters x (for zx) and y (for yz) indicate the OO that is stable deep inside the Mott regime [7].

is the electron number for the d_{xy} orbital of site j. We also assume a value of $\Delta > 0$ that is large enough to localize one electron in the d_{xy} orbital. H_U contains the terms originated from the Coulomb repulsion between electrons in the same ion. When restricted to the $n_{j\,xy} = 1$ subspace, H_U reads

$$\begin{aligned} H_U = & \sum_{j,\mu} [-2J\mathbf{S}_{j\mu} \cdot \mathbf{S}_{j\,xy} + U n_{j\mu\uparrow} n_{j\mu\downarrow}] \\ & + (U-2J) \sum_{j,\mu\neq\nu} n_{j\mu\uparrow} n_{j\nu\downarrow} + \frac{U-3J}{2} \sum_{j,\alpha,\mu\neq\nu} n_{j\mu\alpha} n_{j\nu\alpha} \\ & + J \sum_{j,\mu\neq\nu} \left[d^\dagger_{j\mu\uparrow} d^\dagger_{j\mu\downarrow} d_{j\nu\downarrow} d_{j\nu\uparrow} - d^\dagger_{j\mu\uparrow} d_{j\mu\downarrow} d^\dagger_{j\nu\downarrow} d_{j\nu\uparrow} \right]. \end{aligned} \tag{1}$$

Here U denotes the Coulomb repulsion between electrons occupying the same orbital and J is the Hund's coupling constant [18]. $\mu, \nu = \{zx, yz\}$ are orbital indices, while $\alpha, \beta = \uparrow, \downarrow$ are spin indices. Finally, $n_{j\mu\alpha} = d^\dagger_{j\mu\alpha} d_{j\mu\alpha}$, $n_{j\mu} = \sum_\alpha n_{j\mu\alpha}$, and $\mathbf{S}_{j\mu} = \frac{1}{2} \sum_{\alpha,\beta} d^\dagger_{j\mu\alpha} \boldsymbol{\sigma}_{\alpha\beta} d_{j\mu\beta}$, where $\boldsymbol{\sigma} = (\sigma^x, \sigma^y, \sigma^z)$ is a vector of Pauli matricies. The kinetic energy terms are

$$H_t = \sum_{jj'} \sum_{\mu,\nu,\alpha} t^{\mu\nu}_{jj'} (d^\dagger_{j\mu\alpha}\, d_{j'\nu\alpha} + \text{H.c.}) \tag{2}$$

We assume that the transfer matrix is diagonal in the t_{2g} manifold and that the hopping integral is dominated by the $dd\sigma$ contribution: $t^{\mu\nu}_{jj'} = t^{\mu\mu}_{jj'} \delta_{\mu,\nu}$.

Finally, the effective SO contribution H_{so} is obtained by projecting the original SO interaction, $\lambda \mathbf{L} \cdot \mathbf{S}$, onto the doublet of $\{d_{zx}, d_{yz}\}$ orbitals [19]:

$$H_{so} = i\lambda \sum_{j\alpha} \sigma^z_{\alpha\alpha} \left(d^\dagger_{j\,zx\,\alpha} d_{j\,yz\,\alpha} - d^\dagger_{j\,yz\,\alpha} d_{j\,zx\,\alpha} \right). \tag{3}$$

The SO coupling also contains terms, like $\lambda d^\dagger_{j\,xy\uparrow} d_{j\,\mu\downarrow}$, which mix the d_{xy} with d_{zx} or d_{yz} orbitals. Since these terms are of order λ/Δ, they will be neglected in the following discussion.

A single helical chain ($\lambda = 0$ limit). We now consider a single helical chain that propagates along z-direction with alternating zx and yz bonds. (We use the short notation "μ-bond" for bonds oriented along the μ direction, where $\mu = \{xy, yz, zx\}$.) The hopping matrix elements along each helical chain are $t^{zx,zx}_{j,j+1} = t$ and $t^{yz,yz}_{j,j+1} = 0$ for zx-bonds, $t^{yz,yz}_{j,j+1} = t$ and $t^{zx,zx}_{j,j+1} = 0$ for yz-bonds, while there is no hopping between d_{xy} orbitals. The resulting single-chain hopping Hamiltonian is

$$t \sum_{j\in\text{odd},\,\alpha} \left(d^\dagger_{j+1\,zx\,\alpha} d_{j\,zx\,\alpha} + d^\dagger_{j-1\,yz\alpha} d_{j\,yz\,\alpha} + \text{H.c.} \right). \tag{4}$$

The total charge in each pair of orbitals connected by a finite hopping amplitude is conserved for $\lambda = 0$. This local U(1) invariance of $H(\lambda = 0)$ makes the model quasi-exactly solvable. For realistic Hamiltonian parameters, the ground state of $H(\lambda = 0)$ is always in the fully polarized subspace $\mathcal{S}$ with exactly one electron per bond. The projection of $H(\lambda = 0)$ onto this invariant subspace is mapped into a quantum Ising model (QIM):

$$P_{\mathcal{S}} H(\lambda = 0) P_{\mathcal{S}} = -\mathcal{J} \sum_j \left[\tau^z_{j,j+1} \tau^z_{j+1,j+2} - g \tau^x_{j,j+1} \right], \tag{5}$$

up to a constant $C = N_s(U-J)/4$. Here $\mathcal{J} = (U-3J)/4$, $g = 4t/(U-3J)$, and N_s is the total number of V^{3+} ions in the chain. The Ising variable $\tau^z_{j,j+1}$ is equal to 1 if an electron occupies the right site $(j+1)$ of the bond and -1 if it occupies the left site (j).

The operator that is associated with the local orbital order parameter, $n_{j\,zx} - n_{j\,yz}$, has the following expression in terms of the Ising variables:

$$n_{j\,zx} - n_{j\,yz} \;=\; \pm \frac{\tau^z_{j\pm1,j\pm1+1} + \tau^z_{j,j+1}}{2}, \tag{6}$$

where the $+$ $(-)$ sign holds for odd (even) values of j. The 1D QIM is exactly solvable and the ground state has FM ordering for $U - 3J \geq 4t$. The corresponding order parameter is: $\langle \tau^z_{k=0} \rangle = \sum_j \langle \tau^z_{j,j+1} \rangle$. According to Eq. (6), FM ordering of the Ising variables corresponds to AFO ordering of the original variables:

$$\mathcal{O}_\pi = \frac{1}{L} \sum_j e^{i\pi j} \langle n_{j\,zx} - n_{j\,yz} \rangle = -\langle \tau^z_{k=0} \rangle, \tag{7}$$

where L is the number of sites in the helical chain. Therefore, the quantum phase transition between the FM and

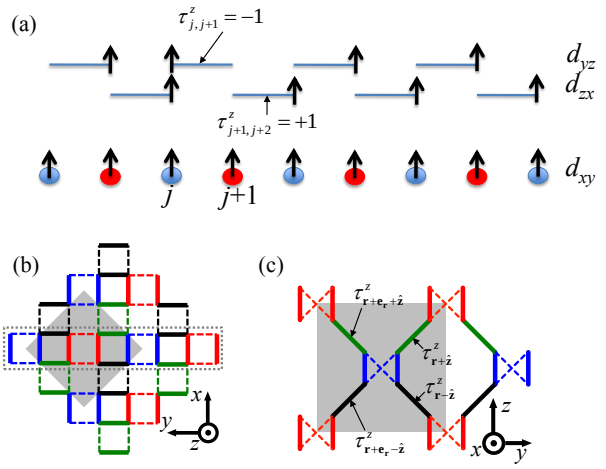

FIG. 2: (Color online) (a) Mapping between $H_{\lambda=0}$ and the QIM. The even and odd sublattices are indicated with blue and red circles respectively. (b) and (c) show the projections of the pyrochlore lattice and the helicoid Ising chains (solid lines) on the xy and yz planes, respectively.

paramagnetic (PM) states of the Ising variables corresponds to AFO-PO transition in terms of the original variables.

The quantum critical point (QCP) occurs at $t = t_c = (U - 3J)/4$ or $|g| = 1$. The exact value of the nearest-neighbor correlator at the QCP is $\langle \tau^z_{j,j+1}\tau^z_{j+1,j+2}\rangle_c = 2/\pi$, which implies a rather low probability of double-occupancy: $\langle n_{j\,zx} n_{j\,yz}\rangle_c = \frac{1}{4}\left(1 - \langle \tau^z_{j,j+1}\tau^z_{j+1,j+2}\rangle_c\right) \simeq 0.09$. This means that the transition to the PO state occurs far from the covalent regime and the inter-chain orbital coupling can be treated as a perturbation.

Coupled Chains. Here we will assume that the effective AFM coupling between chains stabilizes the magnetically ordered state shown in Fig.1. This assumption is supported by unbiased numerical simulations of the three-band Hubbard model that will be presented elsewhere [20]. In addition, this magnetic ordering is stable near the itinerant [21] and strong-coupling limits [7] indicating that it remains stable over the whole Mott phase. Since charge fluctuations are weaker across AFM bonds (the barrier is U instead of $U - 3J$), the coupling between neighboring helical Ising chains [Fig. 2(c)] will be approximated by using a Kugel-Khomskii Hamiltonian [7, 9, 17]. There are two contributions. The first contribution comes from exchange between electrons localized in the d_{xy} orbitals and leads to a pure AFM spin coupling:

$$H_{\rm spin} = J_S \sum_{(ij)} \mathbf{S}_i \cdot \mathbf{S}_j, \qquad (8)$$

where $J_S = \frac{t^2}{U}\frac{1+\eta}{1+2\eta}$ is the spin exchange constant, $\eta = J/U$, (ij) denotes an $\pm xy$-bond which connects two sites belonging to nearest-neighbor Ising chains, and $\mathbf{S}_j = \sum_\gamma \mathbf{S}_{j\gamma}$. The above AFM coupling between helical chains is unfrustrated and leads to the $\mathbf{q} = 2\pi(001)$ 3D magnetic order depicted in Fig. 1.

The second contribution comes from orbital exchange through the antiferromagnetic zx and yz bonds (dashed bonds in Fig. 1) connecting nearest-neighbor Ising chains. The small probability of double occupancy induced by inter-chain hopping processes justifies our perturbative treatment of these terms. The resulting inter-chain orbital Hamiltonian is

$$H_{\rm orb} = \sum_{\langle ij\rangle} K_1 n_{i\mu} n_{j\mu} + K_2\left[n_{i\mu}(1-n_{j\mu}) + (1-n_{i\mu})n_{j\mu}\right], \qquad (9)$$

where $\mu = zx$ (yz) when $\langle ij\rangle$ is a zx (yz)-bond, $K_1 = -2\frac{t^2}{U}\frac{1+\eta}{1+2\eta}$ and $K_2 = -\frac{t^2}{U}\frac{1-2\eta}{1-3\eta}$ denote the FO and AFO couplings.

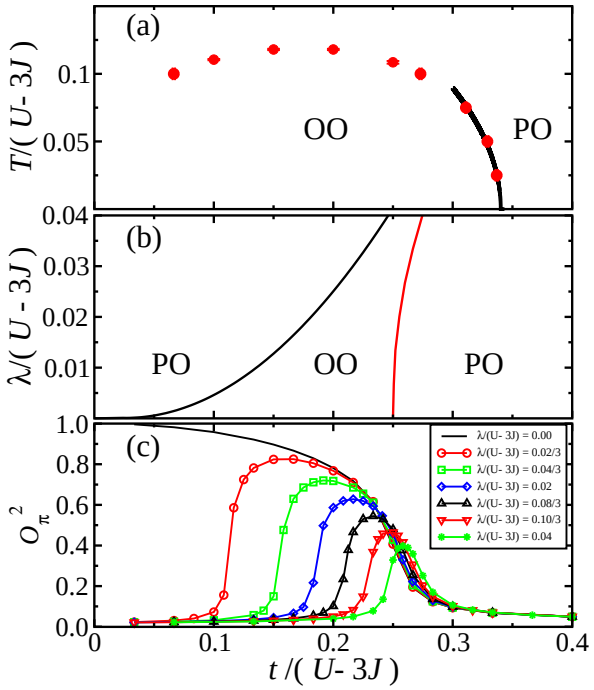

FIG. 3: (Color online) (a) Phase diagram of the three-dimensional quantum Ising model Eq. (10) for $\eta = 0.229$. (b) $T = 0$ (λ, t) phase diagram of the single helical chain Hamiltonian H obtained with DMRG applied to chains of 48 unit cells. (c) Square of the staggered orbital order parameter as a function of t.

A 3D effective Ising Hamiltonian can be easily obtained from Eqs.(5) and (9). The intra-chain term is given by Eq.(5), while the inter-chain coupling is obtained by expressing the orbital occupation operators of Eq. (9) in terms of the Ising variables $n_{j\mu} = (1 \pm \tau^z_{j,j+1})/2$. However, we should recall that the Ising operators are bond variables defined on a dual lattice (see Fig. 2(a)). Therefore, we introduce the bond coordinates $\mathbf{r} = (m, n, j)$ to define the full dual lattice, including the zx and yz-bonds connecting different helical chains. The last coordinate j denotes the position of the bond on its helical chain,

while m and n correspond to the (x, y) chain coordinates. (See Fig. 2.) The resulting quantum Ising Hamiltonian is

$$H_{\rm eff} = -\frac{U-3J}{4}\sum_{\mathbf{r}}\left(\tau^z_{\mathbf{r}+\hat{\mathbf{z}}}\,\tau^z_{\mathbf{r}} - g\,\tau^x_{\mathbf{r}}\right) - \eta\frac{t^2}{U}\sum_{\mathbf{r}}\left(\tau^z_{\mathbf{r}+\mathbf{e}_{\mathbf{r}}-\hat{\mathbf{z}}}\,\tau^z_{\mathbf{r}+\hat{\mathbf{z}}} + \tau^z_{\mathbf{r}+\mathbf{e}_{\mathbf{r}}+\hat{\mathbf{z}}}\,\tau^z_{\mathbf{r}-\hat{\mathbf{z}}}\right), \quad (10)$$

where $\mathbf{e_r} = (\pm1, 0, 0)$ and $(0, \pm1, 0)$ are vectors connecting the site $\mathbf{r}$ to its neighbors. The inter-chain orbital coupling is much weaker than the intra-chain coupling and both are FM. In the large U/t limit (deep inside the MI phase), the FM coupling between Ising variables leads to the AFO order along dashed zx or yz bonds connecting different helical chains (see Fig. 1). This AFO alignment is in contradiction with naive expectations based on the a single-bond analysis. $|K_1| > |K_2|$ for finite η and the orbital superexchange favors a FO configuration the dashed zx- and yz-bonds. However, the state with FO alignment along dashed bonds is frustrated because half of those bonds would contain pairs of occupied orbitals that are not connected by a finite hopping amplitude. In contrast, the energy gain is the same for every bond of the AFO order shown in Fig. 1.

Fig. 3(a) shows the thermodynamic phase diagram of $H_{\rm eff}$ (10) obtained from quantum Monte Carlo (QMC) simulations on lattices containing up to $8\times8\times40$ unit cells (20480 sites). As in the 1D case, the transition between OO and PO occurs in the crossover region between the strong and intermediate-coupling regimes. As expected, the ordering temperature, $T_{\rm OO}$, increases with U.

Finite SO coupling. To compare two different mechanisms for suppression of the AFO ordering, we return to the original Hamiltonian H on a single helical chain and quantify the effect of a finite SO interaction. We apply the density matrix renormalization group (DMRG) method to a chain of 16 sites and verify that the ground state of H is still a fully polarized ferromagnet for $\lambda \leq 0.05(U-3J)$ in the entire regime parameters that we have been considering here. We project H into the fully polarized subspace $\mathcal{S}$ and split each site of the helical chain into two single-orbital sites. Then we arrange the orbitals in a one-dimensional array $d_{j\,zx}, d_{j\,yz}, d_{j+1\,yz}, d_{j+1\,zx}, ...$ and identify each orbital with an effective site l. The result is an effective spinless fermion model with alternating hopping and nearest-neighbor repulsion:

$$P_{\mathcal{S}}HP_{\mathcal{S}} = \sum_l t(c^\dagger_{2l-1}c_{2l} + \text{H.c.}) + (U-3J)n_{2l}n_{2l+1} + i\lambda(c^\dagger_{2l}c_{2l+1} - c^\dagger_{2l+1}c_{2l}). \quad (11)$$

The ground state of $P_{\mathcal{S}}HP_{\mathcal{S}}$ is obtained by applying DMRG to a chain of 48 sites. The resulting (λ, t) quantum phase diagram and the AFO order parameter $\mathcal{O}_\pi$ [see Eq. (7)] are presented in Fig. 3(b) and (c), respectively. It is clear that SO coupling and charge fluctuations effectively suppress the AFO order in different parts of the phase diagram. SO coupling λ is very effective for suppressing the AFO deep inside the MI (large U) regime. A small SO coupling of about 6% of the Coulomb energy drives the system into the PO state because λ competes against a super-exchange energy scale of order t^2/U that stabilizes the AFO order [8]. On the other hand, SO coupling has little effect in the vicinity of the QCP because the competing energy scale that determines the strength of the charge fluctuations is of order t. We should emphasize that although Fig. 3 includes a region deep inside the MI regime, our approach is quantitatively correct only near the QCP that separates the OO and PO phases.

In summary, our results offer a new perspective for understanding the electronic properties of the vanadium spinels AV_2O_4. While CdV_2O_4 seems to be not too far from the localized or strong-coupling regime, it is not clear if the magnetic ordering is accompanied by OO. Different experimental probes indicate that MgV_2O_4 and ZnV_2O_4 are well inside the intermediate-coupling regime [6, 15, 22]. MgV_2O_4 and ZnV_2O_4 exhibit the same type of $\uparrow\uparrow\downarrow\downarrow$ magnetic ordering and there is no evidence of OO down to the lowest accessible temperatures. According to our calculations, the SO interaction is very effective for suppressing OO in the localized regime relevant for CdV_2O_4 [8]. However, the lack of OO in the intermediate-coupling regime relevant for MgV_2O_4 and ZnV_2O_4 is mainly driven by charge fluctuations and basically insensitive to the magnitude of the SO interaction. While SO still contributes to the rather large suppression of the V^{3+} moment in the three compounds ($1.19\mu_B$ in CdV_2O_4, 0.63 μ_B in ZnV_2O_4 and $0.47\mu_B$ in MgV_2O_4), we attribute the significantly smaller values observed in ZnV_2O_4 and MgV_2O_4 to the same charge fluctuations that suppress the OO.

ZnV_2O_4 and MgV_2O_4 have very similar lattice parameters [6]. The estimated value of t for the cubic phase of ZnV_2O_4 with lattice parameter 2.97 Å is $t \simeq 0.35$ eV [23]. According to our results, the OO should disappear completely for $U - 3J \gtrsim 1.2$ eV. If we assume that $U \simeq 3.5$ eV [15] and $J \simeq 0.8$ eV [7, 10], OO should be completely suppressed in agreement with experimental observations. We note that the PO phase found for $t \geq 0.3(U-3J)$ is similar to the state obtained from an *ab initio* itinerant approach [15]. However, the bond order parameter associated with the $\uparrow\uparrow\downarrow\downarrow$ magnetic ordering is much weaker close to the QCP than in the itinerant regime. In other words, the lattice distortion induced by the bond ordering (FM bonds become shorter than the AFM ones) near the QCP should be much smaller than the value reported in Ref. [15]. This could explain why recent NS measurements have not observed the strong dimerization predicted in Ref. [15]. This may also be the reason why *ab initio* calculations overestimate the electric polarization induced by the same bond ordering in CdV_2O_4 [5]. We believe that much better quantitative agreement can be obtained from an intermediate-coupling treatment, like the one presented here, that incorporates the coupling to the lattice degrees of freedom.

We are grateful to D. Khomskii, F. Rivadulla and V. Pardo for many useful discussions. Work at the LANL was performed under the auspices of the U.S. DOE contract No. DE-AC52-06NA25396 through the LDRD program. A.E.F. thanks NSF for support through Grant No. DMR-0955707. G.W.C. acknowledges the support of ICAM and NSF grant DMR-0844115. N.P. acknowledges the support of NSF grant DMR-1005932.

[1] S.-H. Lee *et al.*, Phys. Rev. Lett. **93**, 156407 (2004).
[2] M. Reehuis, *et al.*, Eur. Phys. J. B **35**, 311 (2003).
[3] E. M. Wheeler *et al.*, Phys. Rev. B **82**, 140406 (2010).
[4] M. Onoda and J. Hasegawa, J. Phys.: Cond. Matt. **15**, L95 (2003)
[5] G. Giovannetti *et al.*, Phys. Rev. B **83**, 060402(R) (2011).
[6] S. Blanco-Canosa *et al.*, Phys. Rev. Lett. **99**, 187201 (2007).
[7] H. Tsunetsugu and Y. Motome, Phys. Rev. B **68**, 060405(R) (2003).
[8] O. Tchernyshyov, Phys. Rev. Lett. **93**, 157206 (2004).
[9] S. Di Matteo, G. Jackeli, and N. B. Perkins, Phys. Rev. B **72**, 020408(R) (2005).
[10] T. Maitra and R. Valenti, Phys. Rev. Lett. **99**, 126401 (2007).
[11] A. Abragam and B. Bleaney, *Introduction to Ligand Field Theory, Clarendon*, Oxford, 1970.
[12] T. Mizokawa and A. Fujimori, Phys. Rev. B **54**, 5368 (1996).
[13] N. B. Perkins and O. Sikora, Phys. Rev. B **76**, 214434 (2007); G.-W. Chern and N. Perkins, Phys. Rev. B **80**, 180409 (R), 2009.
[14] D. Bloch, J. Phys. Chem. Solids 27, 881 (1966).
[15] V. Pardo *et al.*, Phys. Rev. Lett. **101**, 256403 (2008).
[16] Here we will use the word "para-orbital" to denote any phase with no orbital ordering other than the trivial orbital magnetic ordering induced by $\langle \mathbf{S}_i \rangle \neq 0$ and finite spin-orbit coupling.
[17] K. I. Kugel and D. I. Khomskii, Sov. Phys. Usp. **25**, 231 (1982).
[18] E. Dagotto, T. Hotta, and A. Moreo, Phys. Rep. **344**, 1 (2001).
[19] P. Horsch, G. Khaliullin, and A. M. Oleś, Phys. Rev. Lett. **91**, 257203 (2003).
[20] Y. Kato *et al.*, in preparation.
[21] G.-W. Chern and C. D. Batista, Phys. Rev. Lett. **107**, 186403 (2011).
[22] A. Kismarahardja *et al.*, Phys. Rev. Lett. **106**, 056602 (2011).
[23] K. Takubo *et al.*, Phys. Rev. B **74**, 155103 (2006).